Available online at www.sciencedirect.com
ScienceDirect
International Journal of Mass Spectrometry 265 (2007) 106–123
International Journal of Mass Spectrometry
www.elsevier.com/locate/ijms

Proton and hydrogen atom adducts to cytosine. An experimental and computational study

Chunxiang Yao [a], František Tureček [a,*], Michael J. Polce [b], Chrys Wesdemiotis [b]

[a] *Department of Chemistry, Bagley Hall, Box 351700, University of Washington, Seattle, WA 98195-1700, USA*
[b] *Department of Chemistry, University of Akron, Akron, OH, USA*

Received 11 October 2006; received in revised form 20 January 2007; accepted 23 January 2007
Available online 30 January 2007

Abstract

Cytosine cations were generated by chemical ionization and fast-atom bombardment of cytosine, and their dissociations in the gas phase were studied by tandem mass spectrometry and quantum chemistry calculations at levels of theory up to CCSD(T)/aug-cc-pVTZ. Metastable cytosine cations undergo loss of NH_3, H_2O, and [CHNO] molecules as major dissociations. Mechanisms for these dissociations were established by a combination of MS^3, deuterium labeling, and calculations. Several tautomers of protonated cytosine were identified to exist as local energy minima. The tautomers are predicted to undergo facile prototropic isomerizations at internal energies below the lowest ion-dissociation thresholds. The lowest-energy elimination of ammonia proceeds from open-ring structures and is accompanied by exchange of the N-3 and N-7 positions in cytosine, so that either nitrogen atom can be lost in the ammonia molecule. Cytosine radicals corresponding to hydrogen atom adducts are stable when formed by femtosecond electron transfer to the cations. A fraction of the radicals dissociate by loss of hydrogen atom to form cytosine tautomers. Ring-cleavage dissociations leading to the loss of CO and HNCO are less abundant, and are predicted to proceed from excited electronic states accessed by vertical electron transfer.

Keywords: Cytosine; Protonation; Ion tautomers; Proton affinities; Radicals

1. Introduction

Hydrogen atom adducts to nucleobases are important transient radical intermediates in the complex process of DNA radiation damage [1]. In our previous studies, we have shown that nucleobase radicals can be generated in the gas phase by the reaction sequence shown in Scheme 1 [2,3]. First, the nucleobase is selectively protonated at the desired position by a gas-phase acid of an acidity that matches the topical proton affinity of the basic center in the neutral nucleobase, and the cation is characterized by the methods of gas-phase ion chemistry. Second, the cations are accelerated to a high velocity, typically 100,000–200,000 m s^{-1} corresponding to a 7–8 keV kinetic energy, and converted to radicals by femtosecond collisional electron transfer from a polarizable atomic or molecular donor, e.g., Xe, CH_3SSCH_3, $(CH_3)_3N$, or *N*,*N*-dimethylaniline. Radical fragmentations are elucidated by mass spectrometric analysis of products following non-selective collisional ionization. This neutralization–reionization mass spectrometric (NRMS) method [4] allows one to study transient intermediates using cations or anions as charged precursors, and to detect the products of radical dissociations as cations or anions [5]. NRMS has been used previously to generate and study radicals derived from the nucleobases uracil [6–8], adenine [9], and 1-methylcytosine [10]. A common feature of the first two systems was that the parent nucleobases could be obtained in the gas-phase as one dominant tautomer that was selectively protonated to yield a single ion tautomer. With 1-methylcytosine, selective protonation was impossible in the gas phase because of the virtually identical gas-phase basicities of N-3 and O-2 in the molecule [11]. Cytosine represents an even more challenging system in that both the neutral molecule and the protonated cation can exist as several tautomers. In this work we report a combined experimental and computational study aimed at disentangling the intricacies of gas-phase ion chemistry of protonated cytosine and gaining information on the dissociations of cytosine radi-

* Corresponding author. Tel.: +1 206 685 2041; fax: +1 206 685 3478.
E-mail address: turecek@chem.washington.edu (F. Tureček).

1387-3806/$ – see front matter © 2007 Elsevier B.V. All rights reserved.
doi:10.1016/j.ijms.2007.01.013

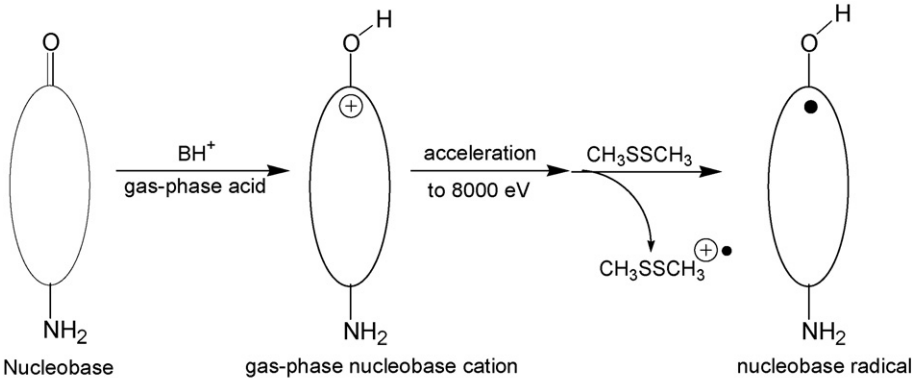

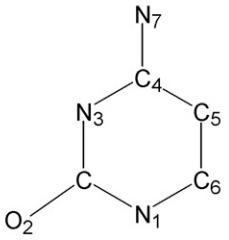

Scheme 1.

cals produced from protonated cytosine upon collisional electron transfer.

2. Experimental

2.1. Materials and methods

Cytosine (Sigma–Aldrich) was used as received and sampled to the mass spectrometers from a heated solid probe or using fast atom bombardment with sulfuric acid as matrix [12]. Metastable-ion and collisionally activated dissociation (CAD) mass spectra (collisions with He, O_2, Ar, and trimethylamine) of cytosine ions produced by FAB were obtained as kinetic energy and mass-resolved scans on a VG-Autospec tandem mass spectrometer operating at 8 keV [13]. Collisionally activated dissociation spectra of cytosine ions produced by chemical ionization were measured on a JEOL HX-110 double focusing mass spectrometer of EB geometry (electrostatic analyzer E precedes magnetic sector B). Air was admitted to the first field free region at pressures to achieve 70% or 50% transmittance of the precursor ion beam at 10 keV. The CAD spectra were recorded by scanning E and B while maintaining a constant B/E ratio (B/E linked scan). The mass resolution in these linked scans was >500. Neutralization–reionization ($^+NR^+$) mass spectra were measured on the VG-Autospec tandem mass spectrometer at 8 keV ion kinetic energy. Ions were prepared by FAB from sulfuric acid or D_2SO_4 matrices, selected by mass, and neutralized by collisions with trimethylamine at 80% ion beam transmittance. The remaining ions were deflected away from the beam, and the neutrals were reionized by collisions with oxygen at 80% beam transmittance. The spectra were obtained as kinetic energy scans. Neutral-fragment reionization spectra ($^+N_fR^+$) [14] were obtained by collisions with He, followed by ion deflection and neutral reionization with O_2. $^+NR^-$ and charge-reversal ($^+CR^-$) mass spectra [15] were obtained with trimethyl amine at 80% beam transmittance.

2.2. Calculations

Standard ab initio calculations were performed using the Gaussian 03 suite of programs [16]. Optimized geometries were obtained by density functional theory calculations using Becke's hybrid functional (B3LYP) [17–19] and the 6–31+G(d,p) basis set. Another set of structures for several neutral cytosine tautomers were obtained by optimizations that used the Møller–Plesset theory [20] with all-electron excitations (MP2(FULL)) and the 6–31+G(d,p) basis set. Complete optimized structures of all local minima and transition states can be obtained from the corresponding author (F.T.) upon request. Spin unrestricted calculations were performed for all open-shell systems. Stationary points were characterized by harmonic frequency calculations with B3LYP/6-31+G(d,p) as local minima (all real frequencies) and first-order saddle points (one imaginary frequency). The calculated frequencies were scaled with 0.963 and used to obtain zero-point energy corrections, enthalpies, and entropies. The rigid-rotor harmonic oscillator (RRHO) model was used in thermochemical calculations except for low frequency modes where the vibrational enthalpy terms that exceeded 0.5 RT were replaced by free internal rotation terms equal to 0.5 RT. It has been shown previously that enthalpies and entropies based on the RRHO and free rotation approximations bracket the more accurate values calculated with the hindered internal rotor model [21], and the small differences cancel out

in calculations of relative enthalpies and entropies. Improved energies were obtained by single-point calculations that were carried out at several levels of theory, including split-valence triple-ζ basis sets of increasing size furnished with polarization and diffuse functions, e.g, 6-311G(d,p), 6-311+G(3df,2p), 6-311++G(3df,2p), 6-311G(3df,2pd), 6-311++G(3df,2pd), and Dunning's correlation consistent basis sets cc-pVTZ and aug-cc-pVTZ [22]. The B3LYP and MP2 energies calculated with the large basis set were combined according to the B3-MP2 scheme, as described previously [23,24]. Single point energies were also calculated with coupled-cluster theory [25] including single, double, and disconnected triple excitations (CCSD(T)) [26] and the 6–31G(d,p) and 6–311G(d,p) basis sets. These were then extrapolated to effective CCSD(T)/6-311+G(3df,2p), CCSD(T)/6-311++G(3df,2p),and CCSD(T)/6-311G(3df,2pd) and CCSD(T)/6-311++G)3df,2pd), using the standard formula (Eq. (1))

$$E[\text{CCSD(T)/large basis set}] \cong E[\text{CCSD(T)/small basis set}] + E[\text{MP2/large basis set}] - E[\text{MP2/small basis set}] \quad (1)$$

For selected systems, large-scale single point CCSD(T) calculations were also carried out with the cc-pVTZ and aug-cc-pVTZ basis sets.

3. Results and discussion

3.1. Cation dissociations

Cations produced by FAB of cytosine solutions and by chemical ioinization of gaseous cytosine with NH_3/NH_4^+ and acetone/$(CH_3)_2COH^+$ were characterized by metastable-ion (MI) and CAD mass spectra. Regardless of the ion preparation mode, the MI spectra showed peaks at *m/z* 95 (loss of ammonia), *m/z* 94 (loss of water), *m/z* 69 (loss of [CHNO], no structure implied), and *m/z* 18 (NH_4^+) (Fig. 1a). Formations of these fragments represent the lowest-energy dissociations of protonated cytosine, as discussed below with the help of theoretical calculations. Collisional activation of protonated cytosine resulted in additional dissociations by loss of H (*m/z* 111), combined loss of CO and HCN (*m/z* 57), and consecutive dissociations of the primary fragments forming ions at *m/z* 66–68, 52, 38–44, 30, and 28 (Fig. 1b). The origin of these fragments was established by a combination of deuterium labeling and MS^3 experiments.

Deuterium labeling in cytosine was accompanied by extensive exchange of several hydrogen atoms that occurred in part in solution and in part in the gas phase under CI conditions. For example, the ND_3/ND_4^+-CI mass spectrum of cytosine, in which the labile hydrogen atoms were exchanged for deuterium in solution at neutral pH, showed 2% D_2, 6% D_3, 29% D_4, 43% D_5, and 20% D_6 species, giving the mean deuterium content equal

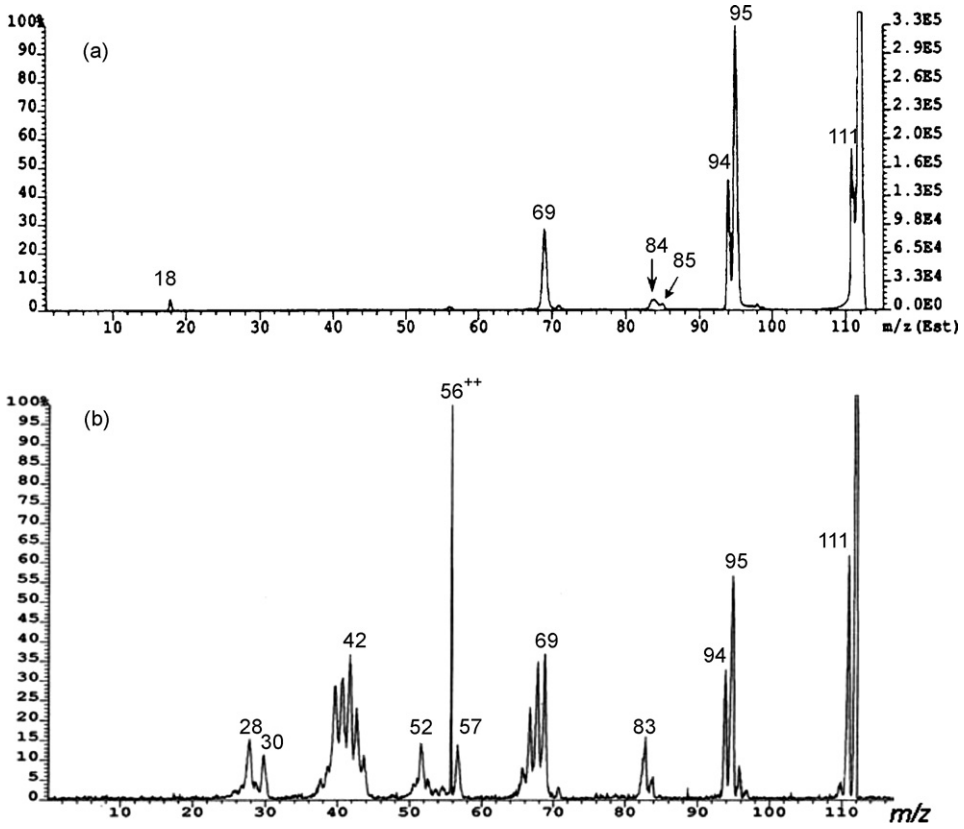

Fig. 1. (a) Metastable-ion spectrum of $(\text{cytosine} + H)^+$ cations at *m/z* 112 prepared by FAB from sulfuric acid matrix. The MI spectrum was obtained as a kinetic energy scan. The shoulder at an apparent *m/z* 111 is an interference from the peak of the much more abundant precursor ion at *m/z* 112. (b) Collisionally activated dissociation (CAD) mass spectrum of 8 keV $(\text{cytosine} + H)^+$ cations at *m/z* 112 prepared by FAB ionization from a sulfuric acid matrix. O_2 was used as a collision gas at 80% ion beam transmittance (*T*). The CAD mass spectrum was obtained as a mass-resolved linked scan.

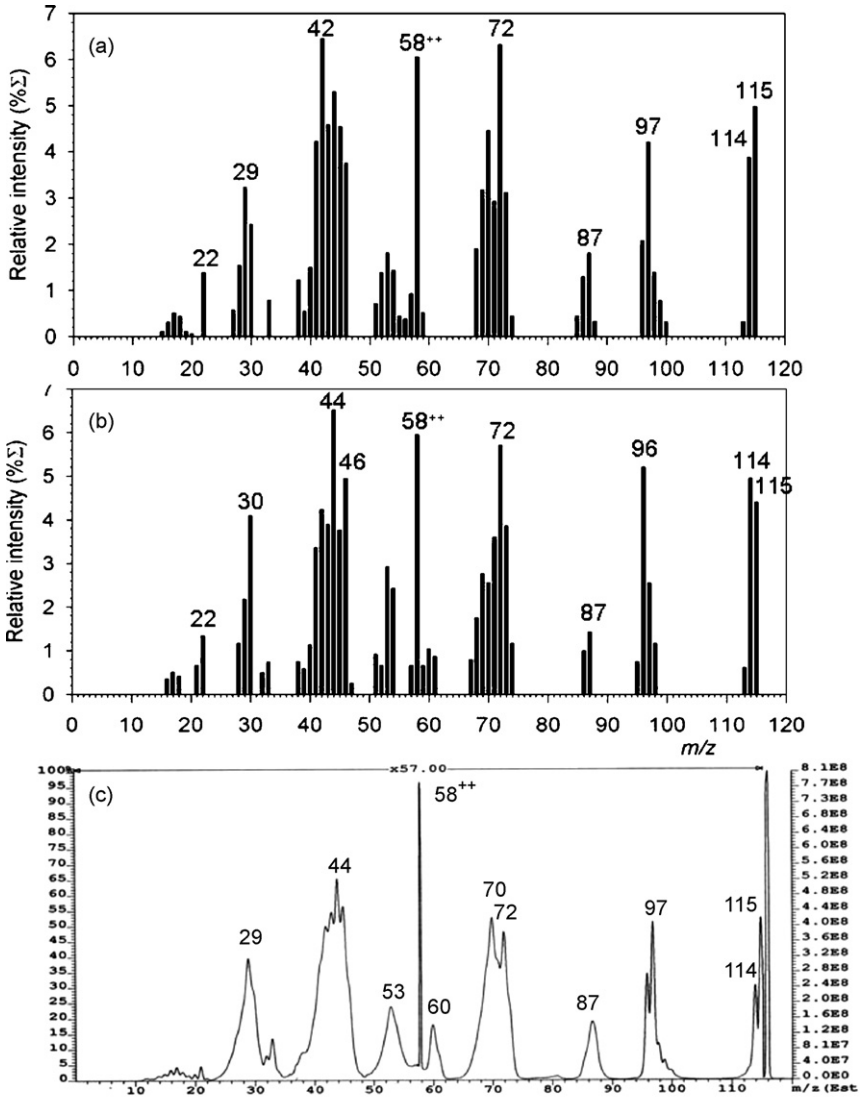

Fig. 2. CAD spectra of [cytosine-d_3 + D]$^+$ ions at *m/z* 116 prepared by (a) acetone-d_6/$(CD_3)_2C{-}OD^+{-}CI$, (b) $ND_3/ND_4^+{-}CI$, and (c) FAB ionization from a D_2SO_4 matrix.

to $\alpha_D = 0.787$ [27]. The experimental deuterium distribution was not far from the statistical one for the same α_D, which was calculated as 2% D_2, 9% D_3, 26% D_4, 39% D_5, and 24% D_6 species. This indicated that all six protons in the cytosine ion were susceptible to exchange in neutral solution followed by ND_3/ND_4^+-CI. The CAD spectra of [cytosine-d_3 + D]$^+$ ions at *m/z* 116 prepared by acetone-d_6/$(CD_3)_2COD^+$ and ND_3/ND_4^+-CI differed in mass shifts of some fragments (Fig. 2a,b, respectively), whereby the former spectrum was quite similar to that of the *m/z* 116 ion produced by FAB from the D_2SO_4 matrix (Fig. 2c). For example, the Fig. 2a and c spectra showed a more abundant loss of H versus D, while an opposite ratio was observed in Fig. 2b. Noteworthy is the prominent loss of ND_2H/HDO (*m/z* 97) from ions made by acetone-d_6/CI and FAB, as opposed to loss of ND_3 /D_2O (*m/z* 96) from those made by ND_3/ND_4^+-CI. The peak for elimination of [CHNO] (*m/z* 69 in Fig. 1b) is shifted to *m/z* 72 and 73 in the CAD spectra of [cytosine-d_3 + D]$^+$. Since *m/z* 73 corresponds to elimination of [CHNO] containing a light hydrogen atom, the dissociation must have involved a H/D exchange between the nominally acidic positions N-1, O-2, N-3 and N-7 and the nominally non-acidic ones at C-5 and C-6. We note in this context, that the hydrogen at C-5 is susceptible to H/D exchange in solution, as reported recently for 1-methylcytosine [11]. The fragments of the *m/z* 36–46 group retain more deuterium atoms when formed from the [cytosine-d_3 + D]$^+$ ion prepared by ND_3/ND_4^+-CI. The ion at *m/z* 57 showed mass shifts of 3–4 u when formed from the [cytosine-d_3 + D]$^+$ cation at *m/z* 116. This indicated that the neutral fragments eliminated in this dissociation could contain a maximum of one hydrogen atom, which logically led to the combined loss of CO and HCN. Overall, the CAD spectra of the deuterium-labeled ions indicated substantial H/D exchange in the parent compounds and ions, and possibly also in the course of dissociation.

MS^3 of the *m/z* 95 fragment produced from metastable [cytosine + H]$^+$ (Fig. 3a) gave rise to ions at *m/z* 94 (loss of H), 67 (loss of CO), 52, 40 (loss of CO and HCN), and 28 that also

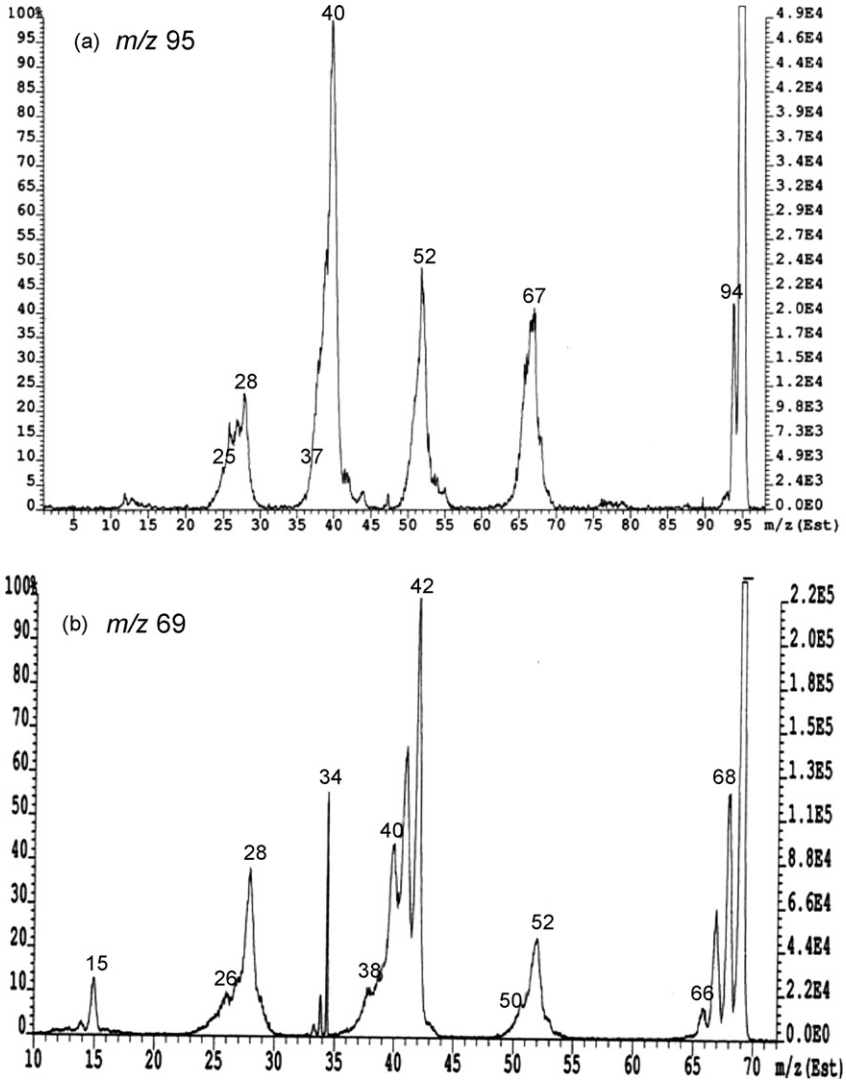

Fig. 3. CAD spectra of (a) *m/z* 95 and (b) *m/z* 69 fragment ions from dissociation of metastable [cytosine + H]$^+$. O_2 was used as a collision gas at 80% main beam transmittance (*T*).

appeared in the CAD spectrum of [cytosine + H]$^+$. Likewise, MS^3 of metastably produced *m/z* 69 ion (Fig. 3b) gave rise to ions at *m/z* 68–66 (losses of H atoms), 52 (loss of NH_3), 42 (loss of HCN), 41–38, and 28. The presence of these fragments in the CAD mass spectrum of [cytosine + H]$^+$ can be in part accounted for by consecutive dissociations of the first-generation fragments. Although the MS^3 spectra were useful in helping to disentangle the dissociations of [cytosine + H]$^+$, alone they did not allow us to assign definite structures to the primary fragment ions.

3.2. Cation energetics

Further insight into the ion chemistry of protonated cytosine was obtained from ab initio and density functional theory calculations of the relative stabilities of [cytosine + H]$^+$ ions and the topical proton affinities in cytosine. Cytosine exists in the gas phase as a mixture of four tautomers, the major components being the *anti* and *syn*-2-hydroxy-4-aminopyrimidines (***I*** and ***II***, respectively, Scheme 2) [28,29]. The other cytosine tautomers (***V–IX***, Scheme 2) are not important for ion formation by protonation, but may occur as products of radical dissociations, as discussed below.

Protonation of the four main cytosine tautomers ***I–IV*** shows convergent formation of three most stable cations $\mathbf{1}^+$–$\mathbf{3}^+$ (Scheme 2). Ion $\mathbf{2}^+$, which arises by convergent protonation of N-1 in ***II*** and O-2 in ***III***, is the most stable isomer at all levels of ab initio theory used in this work (Table 1). For the numbering of the C, N, and O atoms in cytosine, see Scheme 1. At our highest levels of theory, which was CCSD(T) with the large 6-311++G(3df,2pd) and aug-cc-pVTZ basis sets (Table 1), ion $\mathbf{2}^+$ was more stable than the next isomer $\mathbf{1}^+$ by $\Delta H^\circ_{g,0}(\mathbf{1}^+ \rightarrow \mathbf{2}^+) = -7.1\,\mathrm{kJ\,mol^{-1}}$ and $\Delta G^\circ_{g,298}(\mathbf{1}^+ \rightarrow \mathbf{2}^+) = -6.4\,\mathrm{kJ\,mol^{-1}}$ These $\Delta H^\circ_{g,0}$ and $\Delta G^\circ_{g,298}$ differences are larger than previously calculated with MP4/6–31+G(d,p) [29] and indicate a greater preference for structure $\mathbf{2}^+$ in the gas phase. B3LYP calculations gave much smaller differences between the $\mathbf{1}^+$ and $\mathbf{2}^+$ energies [30], and, given the limited

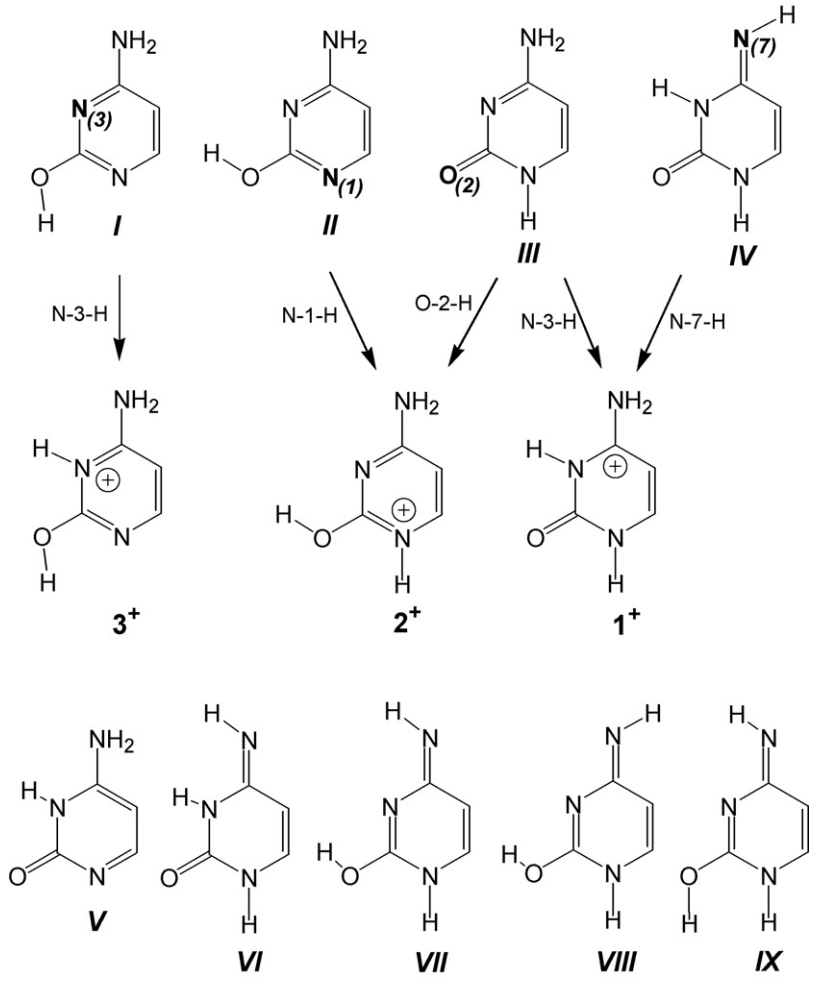

Scheme 2.

reliability of DFT calculations, they would not allow firm conclusions to be made for cytosine cations. Ion $\mathbf{3}^+$, which arises by protonation at N-3 in the most stable neutral cytosine tautomer ***I***, is 30 kJ mol^{-1} less stable than $\mathbf{1}^+$. Six other ion isomers ($\mathbf{4}^+$–$\mathbf{9}^+$) were also evaluated and found to be >100 kJ mol^{-1} less stable than $\mathbf{1}^+$. The optimized structures of ions $\mathbf{1}^+$–$\mathbf{9}^+$ are shown in Fig. 4. The relevance of the various ion isomers will be addressed later in the discussion of ion dissociations.

Although the *relative energies* of protonated cytosine tautomers were consistently reproduced by ab initio calculations at correlated levels of theory, the *topical proton affinities* in cytosine showed an unexpected dependence on the basis set used. Table 2 shows the calculated topical affinities in ***III*** for positions N-3, O-2, N-7, C-5, and C-6. The values for the two most basic positions, O-2 and N-3, show an interesting dependence on the basis set used. In particular, the proton affinities from MP2 and CCSD(T) calculations show conspicuously higher values when calculated with basis sets lacking diffuse functions. This holds even for the large basis sets of triple-ζ quality, cc-pVTZ and 6-311G(3df,2pd), that overestimated the proton affinities by 15–20 kJ mol^{-1} when compared with calculations that used adequate basis sets including diffuse functions, e.g., aug-cc-pVTZ and 6–311+G(3df,2p). Note that deviations of this magnitude are well outside the expected accuracy of CCSD(T) calculations with basis sets of triple-ζ quality [31]. The nature of this effect is not quite clear. Neutral and protonated cytosine are isoelectronic, and thus the deviations must originate from inadequate description of electron distribution in the neutral molecule or cation. Intuitively, inclusion of diffuse functions in the basis set may more affect the calculated distribution of π and σ electron density in the neutral molecules and thus lower their energy and proton affnity. Nevertheless, this example shows that reliable quantum chemistry calculations should be done at several levels of theory using different basis sets and Hamiltonians to recognize and circumvent unexpected deviations.

The calculated topical proton affinities for O-2, N-3, N-7, and C-5 are consistent with the H/D exchange in ND_3/ND_4^+-CI. Exchange is expected when the proton affinity of the site is close to the acidity of the gas-phase acid to allow reversible proton/deuteron transfer [32]. This holds for C-5 (PA = 830 kJ mol^{-1}) and N-7 (PA = 825 kJ mol^{-1}) compared with PA = 853 kJ mol^{-1} for NH_4^+ [33]. However, the fact that all six protons are exchanged in the ND_3/ND_4^+-CI mass spectrum of cytosine is less clear, because the topical proton affinity of C-6 is too low (Table 2). A possible explanation is that exchange at C-6 occurred in solution, and the relative abundance of 6-D-isotopomers was not changed in CI.

Table 1
Relative energies of protonated cytosine tautomers

Method	Cation[a,b]								
	1$^+$	**2**$^+$	**3**$^+$	**4**$^+$	**5**$^+$	**6**$^+$	**7+**	**8**$^+$	**9**$^+$
B3LYP/6-31+G(d,p)	0	−1.0	34	135	128	336	116	310	130
B3LYP/6-311++G(3df,2p)	0	−0.2	35	139	128	339	118	313	134
B3LYP/cc-pVTZ	0	0.0	35						
B3LYP/aug-cc-pVTZ	0	0.3							
MP2/6-31G(d,p)	0	−1.8	35	120	124	364	121	326	109
MP2/6-311G(d,p)	0	−3.7	34						
MP2/6-311G(3df,2pd)	0	−5.8	31						
MP2/6-311+G(3df,2p)	0	−5.1	32						
MP2/6-311++G(3df,2p)	0	−4.7	32	121	125	362	126	323	109
MP2/6-311++G(3df,2pd)	0	−6.6	31						
MP2/cc-pVTZ	0	−6.7	30						
MP2/aug-cc-pVTZ	0	−7.2	30						
B3-MP2/6-311++G(3df,2p)	0	−2.5	34	130	126	351	122	318	122
B3-MP2/cc-pVTZ	0	−3.4							
B3-MP2/aug-cc-pVTZ	0	−3.4							
CCSD(T)/6-31G(d,p)	0	−2.7	34	124	118	343	110	321	115
CCSD(T)/6-311G(d,p)	0	−4.2	33						
CCSD(T)/6-311G(3df,2pd)[c]	0	−6.3	31						
CCSD(T)/6-311+G(3df,2p)[d]	0	−5.6	32						
CCSD(T)/6-311++G(3df,2p)[e]	0	−5.7	32	125	119	341	115	319	115
CCSD(T)/6-311++G(3df,2pd)[f]	0	−7.1	30						
CCSD(T)/cc-pVTZ	0	−6.5	30						
CCSD(T)/aug-cc-pVTZ	0	−7.1	30						
		−6.4[g]	30.3[g]						

[a] Relative energies in units of kJ mol^{-1}.
[b] Including B3LYP/6-31+G(d,p) zero point vibrational corrections and referring to 0 K.
[c] Effective energies from basis set expansion: E[CCSDT)/6-311G(3df,2pd)] = E[CCSDT)/6-311G(d,p)] + E[MP2/6-311G(3df,2pd)] − E[MP2/6-311G(d,p)].
[d] Effective energies from basis set expansion: E[CCSDT)/6-311+G(3df,2p)] = E[CCSDT)/6-311G(d,p)] + E[MP2/6-311+G(3df,2p)] − E[MP2/6-311G(d,p)].
[e] Effective energies from basis set expansion: E[CCSDT)/6-311++G(3df,2p)] = E[CCSDT)/6-31G(d,p)] + E[MP2/6-311++G(3df,2p)] − E[MP2/6-31G(d,p)].
[f] Effective energies from basis set expansion: E[CCSDT)/6-311++G(3df,2pd)] = E[CCSDT)/6-311G(d,p)] + E[MP2/6-311++G(3df,2pd)] − E[MP2/6-311G(d,p)].
[g] $\Delta G^\circ_{g,298}$ values.

3.3. Dissociation mechanisms

The dissociations of metastable cytosine cations and those observed upon collisional activation were also addressed by DFT and ab initio calculations with the goal of elucidating the relevant reaction mechanisms. The dissociation and transition state energies are summarized in Table 3. A conspicuous feature of cytosine ion dissociations is the relatively high threshold energies even for dissociations occurring in metastable ions. Table 3 shows that losses from **1**$^+$ of ammonia, water and [CHNO] molecules require >300 kJ mol^{-1} at their corresponding thermochemical thresholds. This brings up the question of competing prototropic isomerizations of protonated cytosine tautomers **1**$^+$–**4**$^+$, which are addressed first.

3.4. Cation isomerizations

Scheme 3 shows the pathways for prototropic isomerizations of **1**$^+$–**4**$^+$ and **9**$^+$ by competitive and consecutive 1,3-proton migrations. Path ***a*** reversibly isomerizes ions **1**$^+$ and **2**$^+$ through **TS1**. The relevant TS energy, E_{TS1} = 157 kJ mol^{-1} (Table 3) is well below the lowest dissociation threshold. This indicates that isomers **1**$^+$ and **2**$^+$ having internal energies sufficient for dissociation will rapidly interconvert to a form a mixture. Due to the very similar relative energies of **1**$^+$ and **2**$^+$ (Table 1), the dissociating cytosine ions are expected to be in a ∼45:55 ratio of **1**$^+$ and **2**$^+$. A trivial consequence of the isomerization is that isomers **1**$^+$ and **2**$^+$ are indistinguishable by metastable-ion spectra and very difficult to distinguish by CAD. Low (sub-threshold) TS energies were also calculated for 1,3-proton migrations that isomerize **1**$^+$ and **3**$^+$ (path ***b***, E_{TS2} = 187 kJ mol^{-1}), **1**$^+$ and **4**$^+$ (path ***c***, E_{TS3} = 215 kJ mol^{-1}), **3**$^+$ and **9**$^+$ (path ***d***, E_{TS4} = 214 kJ mol^{-1}), **2**$^+$ and **10**$^+$ (path ***e***, E_{TS5} = 240 kJ mol^{-1}), and **3**$^+$ and **10**$^+$ (path ***f***, E_{TS6} = 247 kJ mol^{-1}). Because of their high relative energies, ions **4**$^+$, **9**$^+$, and **10**$^+$ should be considered reactive intermediates of the pertinent dissociations rather than components of tautomeric equilibrium. The loss of water from **10**$^+$ was calculated to be continuously endothermic, as was the loss of ammonia from **4**$^+$ and **9**$^+$ (Scheme 3). Because of the dipolar nature of water and ammonia, it is possible that they form complexes with ions **11**$^+$–**13**$^+$ as shallow potential energy minima along the dissociation pathways, as calculated for other nucleobase cations [34], but these were not studied in detail for cytosine. An interesting feature of the potential energy surface for prototropic isomerizations is the relatively high TS energy for the slightly exothermic proton migration from N-7 to C-5 in **4**$^+$ (Scheme 3, path ***g***, E_{TS7} = 351 kJ mol^{-1}). This is consistent with the differences in the CAD spectra of D-labeled cytosine cations that were pre-

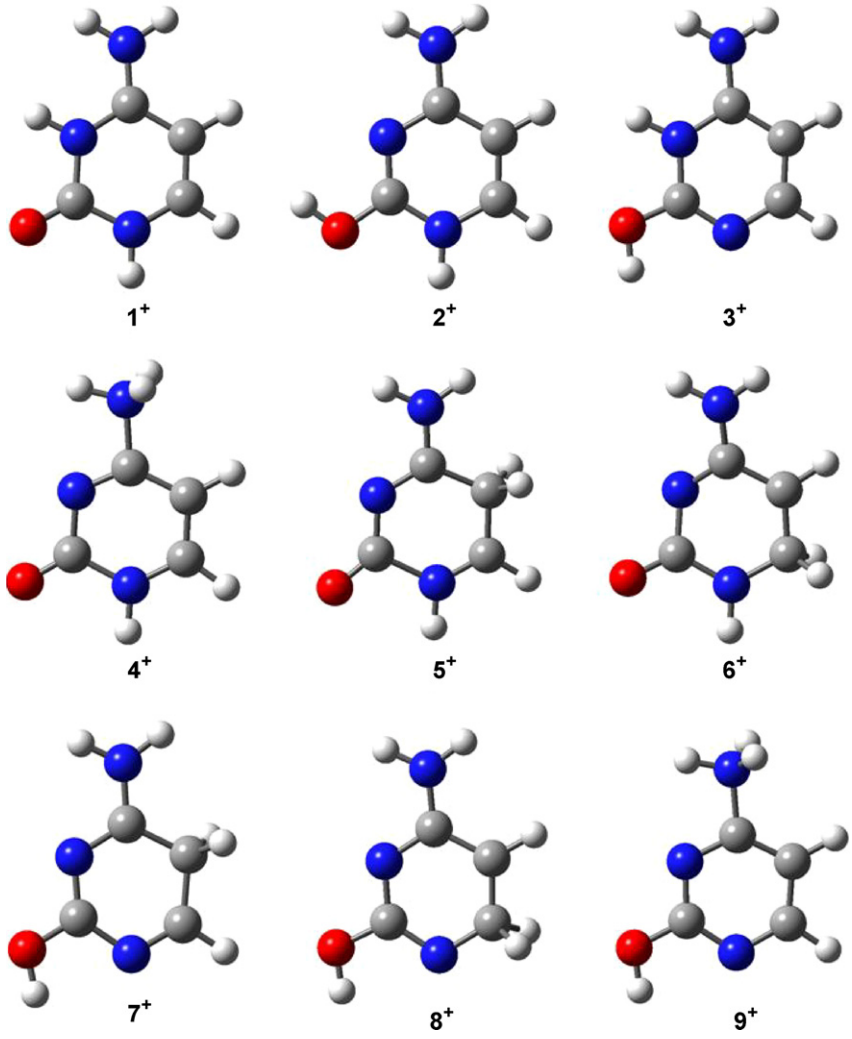

Fig. 4. B3LYP/6-31+G(d,p) optimized structures of [cytosine + H]$^+$ cations **1$^+$**–**9$^+$**.

pared under different CI conditions. Under non-exchanging CI conditions of acetone-d_6/$(CD_3)_2C$–OD^+, the C-5 proton is not exchanged for deuterium in the precursor ion, and its migration following collisional activation is hampered by the high energy required in **TS7**.

3.5. Ring cleavages in cations

In addition to prototropic isomerizations, protonated cytosine shows an important loss of [CHNO] at *m/z* 69 (Fig. 1). An analogous dissociation of protonated 1-methylcytosine has been studied previously [11], and the present discussion follows similar arguments as the previous study. We also note that low-energy CAD of [cytosine + H]$^+$ ions generated from 2′-deoxycytidine produced *m/z* 69 as a major fragment [35]. In addition, the dissociation of a 1,3-^{15}N-labeled cytosine cation showed eliminations of [CH^{15}NO] and [CHNO] in a ∼2:1 ratio that indicated an exchange of the ring and amine nitrogen atoms [35].

We explain this behavior by competing and reversible pathways for ring cleavages and isomerizations leading to elimination of [CHNO] as sumarized in Scheme 4. For the relevant TS energies see Table 3. Cleavage of the N-3–C-2 bond in **1$^+$** proceeds through **TS8** (Scheme 4, path ***h***). Simultaneously with the bond cleavage, the incipient isocyanate group rotates about the N-3–C-4 bond and transfers the N-1 proton on the more basic N-3 in intermediate **14$^+$**. Note that the transition state energy for the ring opening, E_{TS8} = 279 kJ mol^{-1}, is significantly below the dissociation threshold for the loss of ammonia via intermediate **4$^+$** to form ion **11$^+$**. Ion **14$^+$** can undergo degenerate rotation of the protonated amidine moiety about the C-4–C-5 bond, which requires only 24 kJ mol^{-1} in the transition state (**TS9**, E_{TS9} = 94 kJ mol^{-1} relative to **1$^+$**, Table 3). The rotation barrier is mainly due to the the disruption of hydrogen bonding in **TS9**. Note that the rotation effectively exchanges positions N-3 and N-7 in intermediates **14$^+$** and **14′$^+$**, so that either can participate in the elimination of ammonia and [CHNO] through this pathway. Regarding the former dissociation, a recent ^{15}N labeling study reported ∼45% loss of ammonia from N-7 and ∼55% combined loss from N-1 and N-3 [35]. The rate determining step in this pathway for loss of ammonia is a proton migration within the protonated amidine group forming intermediate **15$^+$** via **TS10**

Table 2
Topical proton affinities in the cytosine 2-oxo tautomer ***III***

Method	Proton affinity[a,b]					
	N-3	Syn-O-2	Anti-O-2	N-7	C-5	C-6
B3LYP/6-31+G(d,p)	957	958	923	822	829	620
B3LYP/6-311++G(3df,2p)	958	959	923	820	830	618
B3LYP/cc-pVTZ	969	969	933			
B3LYP/aug-cc-pVTZ	960	961				
MP2/6-31G(d,p)	982	984	947	862	858	617
MP2(FULL)/6-31+G(d,p)	949	953	916			
MP2/6-311G(d,p)	969	973	935			
MP2/6-311G(3df,2pd)	961	967	929			
MP2/6-311+G(3df,2p)	940	946	908			
MP2/6-311++G(3df,2p)	940	945	908	819	814	577
MP2/6-311++G(3df,2pd)	944	951	913			
MP2/cc-pVTZ	956	963	926			
MP2/aug-cc-pVTZ	941	949	911			
B3-MP2/6-311++G(3df,2p)	949	952	915	820	822	598
B3-MP2/cc-pVTZ	963	966				
B3-MP2/aug-cc-pVTZ	951	955				
CCSD(T)/6-31G(d,p)	992	995	957	868	874	647
CCSD(T)/6-311G(d,p)	978	982	945			
CCSD(T)/6-311G(3df,2pd)[c]	970	976	939			
CCSD(T)/6-311+G(3df,2p)[c]	950	955	918			
CCSD(T)/6-311++G(3df,2p)[c]	950	956	918	825	830	607
CCSD(T)/6-311++G(3df,2pd)[c]	953	960	923			
CCSD(T)/cc-pVTZ	967	973	936			
CCSD(T)/aug-cc-pVTZ	952	959	922			
	(918)[d]	(924)[d]	(887)[d]			

[a] In units of kJ mol^{-1}.
[b] Including zero-point and thermal energies and referring to 298 K.
[c] All composite CCSD(T) energies are as defined in Table 1.
[d] Gas-phase basicities at 298 K based on CCSD(T)/aug-cc-pVTZ proton affinities and B3LYP/6-31+G(d,p) entropies.

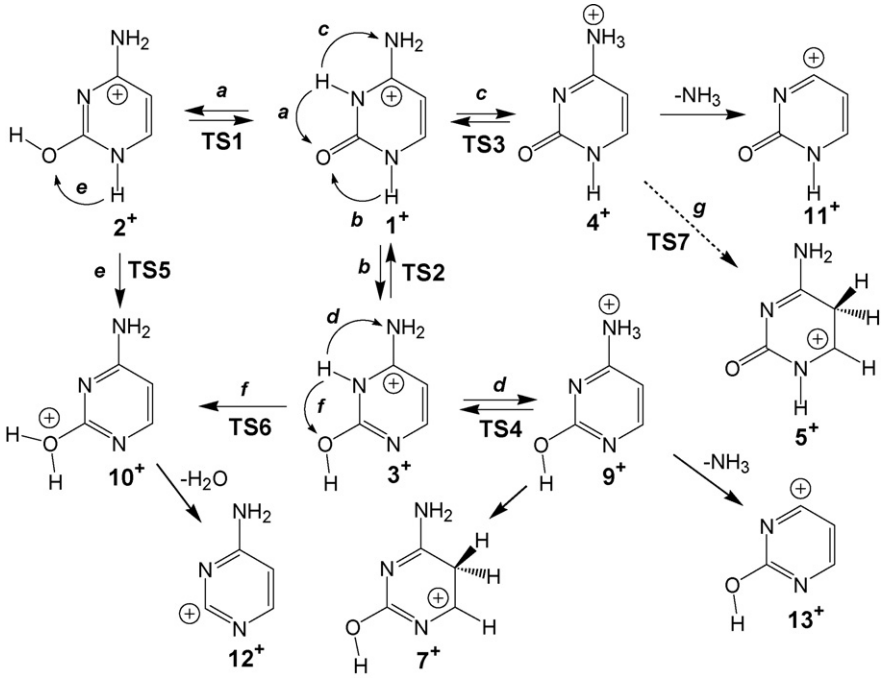

Scheme 3.

Table 3
Dissociation and transition state energies of cytosine cations

Reaction	Energy[a,b]		
	B3LYP 6-31+G(d,p)	B3-MP2 6-311++G(3df,2p)	CCSD(T)[c] 6-311++G(3df,2p)
1$^+$ → **TS1**	157	156	157
1$^+$ → **TS2**	183	184	187
1$^+$ → **TS3**	217	216	215
1$^+$ → **3**$^+$ → **TS4**	220	217	214
1$^+$ → **2**$^+$ → **TS5**	242	239	240
1$^+$ → **3**$^+$ → **TS6**	253	250	247
1$^+$ → **4**$^+$ → **TS7**	352	354	351
1$^+$ → **10**$^+$	191	185	184
1$^+$ → [cytosine ***III***]$^{+\bullet}$ + H$^\bullet$	462	467	472
2$^+$ → [cytosine ***II***]$^{+\bullet}$ + H$^\bullet$	461	466	470
1$^+$ → **11**$^+$ + NH_3	393	379	380
1$^+$ → **12**$^+$ + H_2O	346	336	337
1$^+$ → **13**$^+$ + NH_3	414	406	403
1$^+$ → **TS8**	300	287	279
1$^+$ → **14**$^+$	67	61	70
1$^+$ → **14**$^+$ → **TS9**	97	88	94
1$^+$ → **14**$^+$ → **TS10**	285	280	288
1$^+$ → **15**$^+$	199	188	187
1$^+$ → **16**$^+$ + NH_3	280	264	281
1$^+$ → **TS11**	325	311	303
1$^+$ → **17**$^+$	77	73	88
1$^+$ → **17**$^+$ → **TS12**	363	363	369
1$^+$ → **18**$^+$	254	244	251
1$^+$ → **19**$^+$ + HO—C≡N	322	314	322
1$^+$ → **19**$^+$ + HN=C=O	206	199	219
1$^+$ → **15**$^+$ → **20** + NH_4^+	244	226	231

[a] Energies in units of kJ mol^{-1}.
[b] Including B3LYP/6-31+G(d,p) zero-point energies and referring to 0 K.
[c] Effective energies from basis set expansion: E[CCSDT)/6–311++G(3df,2p)] = E[CCSDT)/6-31G(d,p)] + E[MP2/6-311++G(3df,2p)] − E[MP2/6-31G(d,p)].

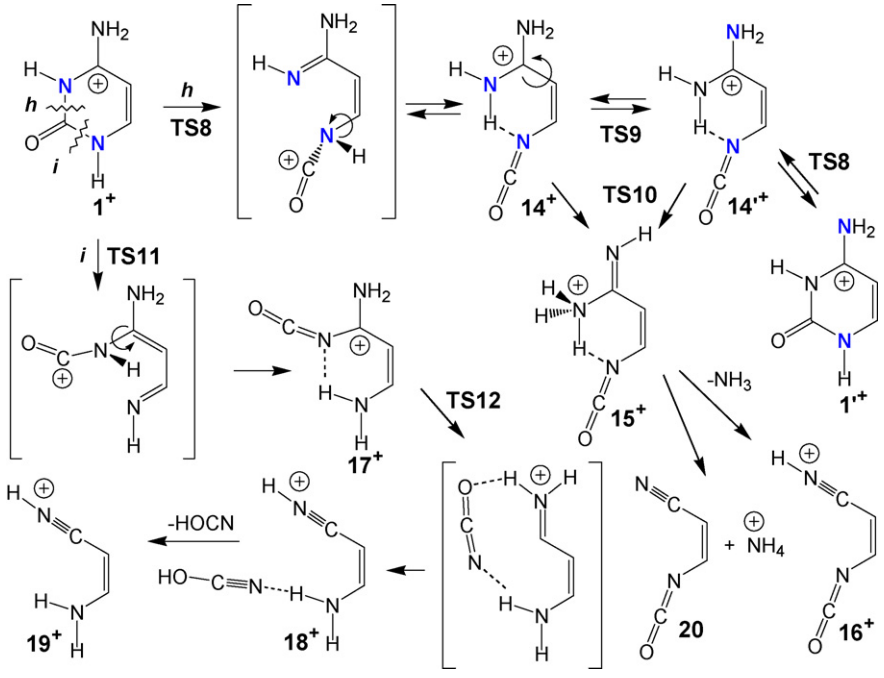

Scheme 4.

(Scheme 4). The thermochemical threshold for the loss of ammonia from $\mathbf{15^+}$ to yield ion $\mathbf{16^+}$ is at 281 kJ mol^{-1} relative to $\mathbf{1^+}$, which is much lower than for the loss through $\mathbf{4^+}$ (380 kJ mol^{-1}, Table 3). Thus, it appears that pathway ***h*** involving ring cleavage is the preferred mechanism for the loss ammonia from $\mathbf{1^+}$, in keeping with experiment [35]. Finally, exothermic proton transfer between $\mathbf{16^+}$ and ammonia can form neutral nitrile **20** and NH_4^+ which was observed as a weak peak in the MI spectrum (Fig. 1a). The data in Table 3 indicate that the proton transfer is 50 kJ mol^{-1} exothermic. The fact that it is not very efficient in metastable-ion dissociations is interesting and cannot be readily explained by dynamic effects. The dissociating system is moving from **TS10** at 288 kJ mol^{-1} through intermediate $\mathbf{15^+}$ to the practically isoenergtic products ($\mathbf{16^+} + NH_3$) at 281 kJ mol^{-1} (Scheme 4). Thus, the NH_3 molecule is not expected to depart with a substantial kinetic energy that would prevent its interaction with the charged product $\mathbf{16^+}$. There is a possibility that the loss of ammonia from intermediate $\mathbf{15^+}$ requires an additional TS energy, but this fine detail was not studied here.

The alternative ring opening in $\mathbf{1^+}$ involves cleavage of the N-1–C-2 bond (Scheme 4, path ***i***). This requires 303 kJ mol^{-1} in **TS11** (Table 3) and also involves proton migration from N-3 to the more basic N-1 in the transition state. Intermediate $\mathbf{17^+}$ is prone to elimination of [CHNO] in two steps. The first step involves dissociation of the N-3–C-4 bond, which is accompanied by the migrating N=C=O fragment forming hydrogen bonds to N-1-H and N-7-H in **TS12**. Further development on the potential energy surface continues with the formation of the OH bond in an ion-molecule complex ($\mathbf{18^+}$) of the incipient fragments, N≡C–OH and $\mathbf{19^+}$. The rate-determining step is the N=C=O migration in **TS12** which requires 369 kJ mol^{-1} relative to $\mathbf{1^+}$ (Table 3). It should be noted that the structure of the [CHNO] neutral fragment has not been determined experimentally. It is possible, albeit not proven, that N≡C–OH isomerizes to the more stable HN=C=O in the ion-molecule complex $\mathbf{18^+}$ [36].

An alternative pathway for [CHNO] elimination is via reversible ring formation, $\mathbf{14'^+} \rightarrow \mathbf{1'^+}$ which now has the former N-7 amine nitrogen atom as N-3. Isomerization through **TS11** and **TS12** in $\mathbf{1'^+}$ can result in an elimination via path ***i*** of [CHNO] that contains N-7. Previous CAD data indicated that this pathway accounted for ∼33% of [CHNO] loss [35] and thus was not kinetically favored. Table 3 energies provide an explanation for this observation. Intermediate $\mathbf{14'^+}$ can undergo a competing isomerization via **TS10** leading to loss of ammonia, or a ring closure to $\mathbf{1'^+}$ via **TS8**. The calculated TS energies (Table 3) show that the isomerization via **TS10** should be preferred. This indicates that the N-7/N-3 exchange should affect the loss of ammonia more than the elimination of [CHNO], as indeed observed. The exact quantitation of these competing dissociations would require a thorough kinetic analysis that was not attempted in this work. We also note that another alternative pathway for [CHNO] elimination via intermediate $\mathbf{15^+}$ cannot be a priori excluded (Scheme 4), but that would require rearrangements to avoid the formation of high-energy $C_3H_5N_2^+$ fragment ions [11].

Finally, loss of a H atom from [cytosine + H]$^+$ is a prominent dissociation that shows low selectivity in D-labeled ions (Fig. 2a–c). Energy data indicate that the losses of H atoms from $\mathbf{1^+}$ and $\mathbf{2^+}$ are high-energy dissociations that require 470–472 kJ mol^{-1} at the pertinent thermochemical thresholds. The fact that the loss of H occurs competitively with the much less endothermic eliminations of ammonia and [C, H, N, O] indicates that it proceeds from an excited electronic state of [cytosine + H]$^+$ that was accessed by collisional excitation at keV kinetic energies [34].

3.6. Cytosine radicals

The protonated cytosine ions produced by FAB were further used to generate cytosine radicals by femtosecond electron transfer from trimethylamine. The neutral intermediates were analyzed after conversion to cations and anions. Also recorded was a neutral-fragment reionization mass spectrum of [cytosine + H]$^+$ to identify neutral fragments produced by collateral CAD. Following reionization, such fragments would appear in the $^+NR^+$ mass spectrum and overlap with fragments of neutral dissociations. The results are summarized in the spectra shown in Fig. 5.

Neutralization of protonated cytosine generates a significant fraction of stable [cytosine + H]$^\bullet$ radicals that are detected as stable cations at *m/z* 112 after collisional reionization (Fig. 5a). The major fragments observed in the $^+NR^+$ mass spectrum arise by losses of H (*m/z* 111), NH_3 (*m/z* 95), H_2O (*m/z* 94), CHO (*m/z* 83), and by ring-cleavage dissociations combined with hydrogen losses (*m/z* 67–69, 51–54, 38–43, 28). Most of these dissociations are also observed in the CAD/TMA spectrum of [cytosine + H]$^+$ (Fig. 5c) and may occur after reionization of stable [cytosine + H]$^\bullet$ radicals. The N_fR mass spectrum (Fig. 5b) shows major peaks of [CHNO] at *m/z* 43 and CO at *m/z* 28, which contribute to the peaks at the same *m/z* in the $^+NR^+$ spectrum. Thus, the main unique features of the $^+NR^+$ mass spectrum are the abundant survivor ion and the fragment due to loss of a hydrogen atom. The $^+NR^+$ mass spectrum of [cytosine-d_3 + D]$^+$ also shows a strong survivor ion (Fig. 6a). Loss of H and D is observed in a 2:3 ratio, which is different from the same ratio in the CAD spectra which show a more abundant loss of H. The other fragments show mass shifts due to the presence of deuterium atoms, e.g., *m/z* 94 and 95 to *m/z* 95–97, *m/z* 83 to *m/z* 86, *m/z* 68 to *m/z* 70, etc. The utility of deuterium labeling for assigning the fragments is somewhat limited by the low mass resolution in the kinetic energy scans that were used to record the $^+NR^+$ mass spectra.

Neutral reionization to anions ($^+NR^-$) did not produce stable survivor anions (Fig. 6b). Since the intermediate radicals are quite stable, as evidenced by the $^+NR^+$ mass spectra, the absence of a survivor peak in the $^+NR^-$ mass spectrum must be due to the instability of [cytosine + H]$^-$ anions. This is corroborated by the charge-reversal mass spectrum ($^+CR^-$) in which the anions are directly generated from the cation in a single collision without the intermediacy of neutral radicals. Fig. 6c shows that the $^+NR^-$ and $^+CR^-$ mass spectra are very similar, indicating that the dissociations that were observed had occurred in the anions.

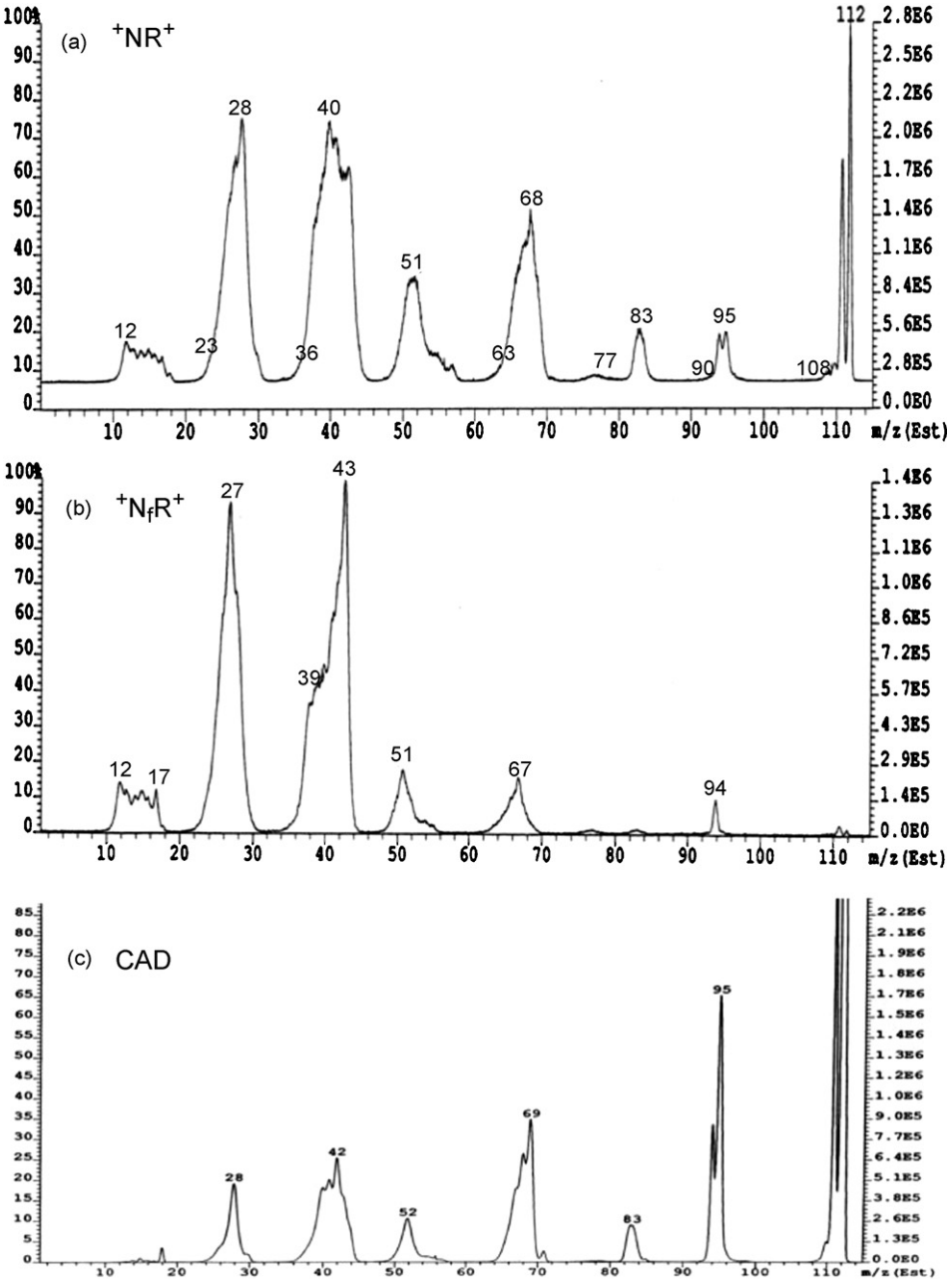

Fig. 5. (a) Neutralization (trimethylamine, 80% *T*)/reionization (O_2, 80% *T*) mass spectrum of [cytosine + H]$^+$ at 8 keV. (b) Neutral-fragment reionization (He/O_2) mass spectrum of [cytosine + H]$^+$. (c) CAD (trimethylamine, 80% *T*) mass spectrum of [cytosine + H]$^+$ at 8 keV.

Our experimental data showing the instability of [cytosine + H]$^-$ anions are in line with recent DFT calculations of adiabatic electron affinities of several (cytosine + H)$^\bullet$ radicals that predicted a very low electron affinity for **1** (0.13–0.27 eV) and negative electron affinities for **2** and **3** [37].

3.7. Radical energetics

The relative and dissociation energies of hydrogen atom adducts to cytosine are summarized in Table 4, and the optimized structures of cytosine radicals are shown in Fig. 7. Detailed geometries of several cytosine radicals, optimized at various levels of theory, have been reported previously [37,38] and need not be discussed here. Radical **1** is the most stable isomer of those we studied. Structure **1** corresponds to an H-atom adduct to the N-3 position in the canonical cytosine tautomer ***III***, and also is an intermediate in collisional electron transfer to ion $\mathbf{1}^+$. The adiabatic ionization energy of **1** was calculated to be $IE_{adiab}(\mathbf{1}) = 5.17$ eV (Table 4). The vertical recombination energy of ion $\mathbf{1}^+$ is $RE_{vert}(\mathbf{1}^+) = 4.72$ eV (Table 4). The $IE_{adiab}(\mathbf{1}) - RE_{vert}(\mathbf{1}^+)$ difference gives an estimate of the mean vibrational excitation in vertically formed **1** (the Franck-Condon energy) as 48 kJ mol^{-1}. The other relevant cytosine radicals are represented by structures **2** and **3** (Fig. 7). Radical **2** can be viewed as a hydrogen atom adduct to O-2 in cytosine ***III***, or to N-1 in cytosine ***II***, and also is an intermediate of electron trans-

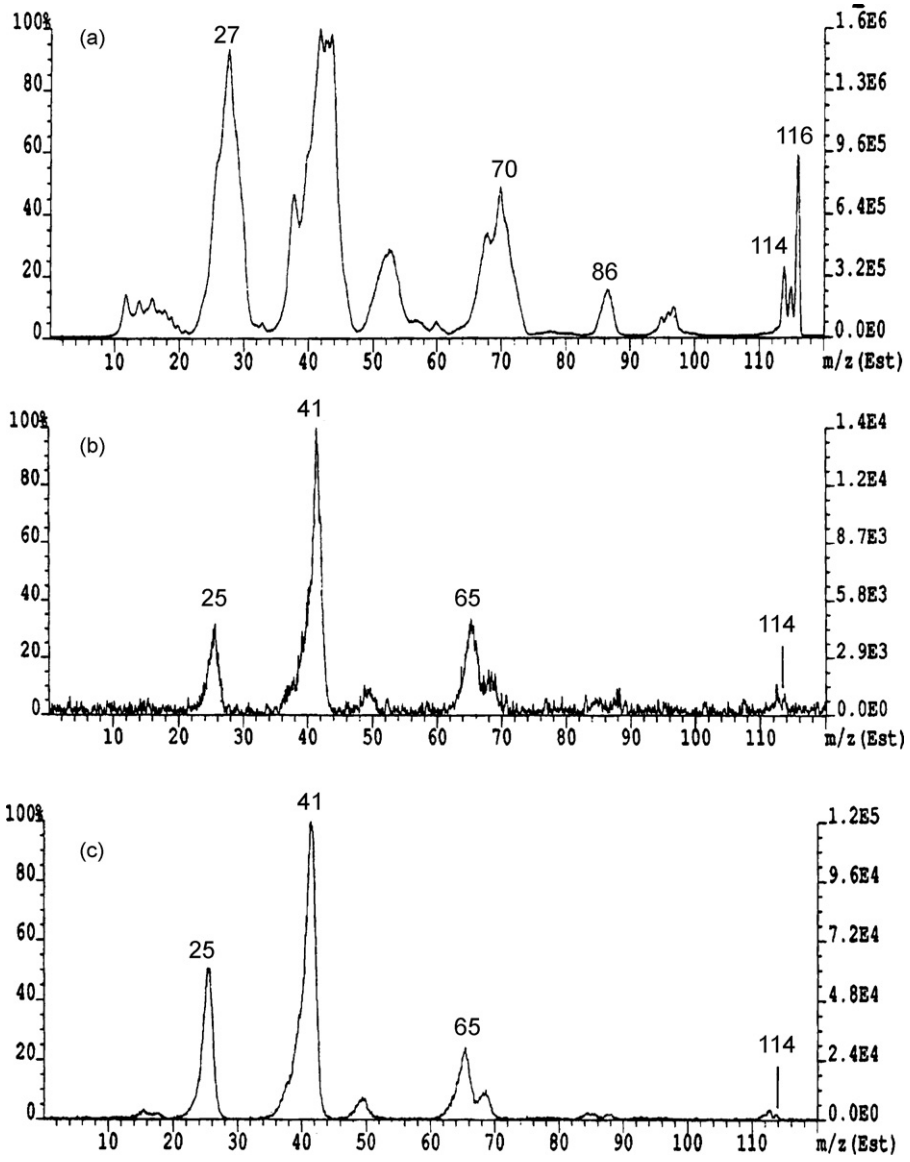

Fig. 6. (a) Neutralization (trimethylamine, 80% T)/reionization (O_2, 80% *T*) mass spectrum of [cytosine-d_3 + D]$^+$ at 8 keV. (b) $^+NR^-$ mass spectrum of [cytosine-d_3 + D]$^+$ at 8 keV. (c) $^+CR^-$ mass spectrum of [cytosine-d_3 + D]$^+$ at 8 keV.

fer to ion **2**$^+$. Radical **3** is a product of H-atom addition to N-3 in cytosine ***I*** and an intermediate from ion **3**$^+$. Radicals **5**, **6**, **7a**, **7b**, **8a**, **8b**, **21**, and **22** are kinetically relevant in H-atom additions to cytosine [38], but their ion precursors are high-energy species (Table 1) that are unlikely to be formed by ionization of cytosine.

A common feature of radicals **5**–**8b** is that their relative energies cluster in a narrow range of 31–71 kJ mol^{-1} above **1**. This indicates that they may be kinetically relevant as intermediates of dissociations of **1**–**3**. Loss of H is an important dissociation of cytosine radicals following collisional electron transfer. The relevant parts of the calculated potential energy surfaces for loss of H from **1** and **2** are shown in Fig. 8. Loss of H-3 from **1** proceeds through a transition state (**TS12**, Fig. 8) that occurs at an N-3–H distance of 1.726 Å. The transition state energy, E_{TS12} = 154 kJ mol^{-1}, is significantly greater than the mean excitation in vertically formed **1** (48 kJ mol^{-1}). This is consistent with the fact that a large fraction of **1** survives following collisional electron transfer (Fig. 5a). Eliminations of other hydrogen atoms from **1**, e.g., those from N-1 and N-7, have not been studied in detail, but their thermochemistry can be readily estimated from the known product relative energies. Dissociation of the *syn* and *anti* N-7–H bonds in **1** would produce cytosines ***IV*** and ***VI*** (Scheme 2) that are slightly less stable than ***III***. Thus, the minimum energy pathways to ***IV*** and ***VI*** are likely to require energies that are similar to or greater than that in **TS12**. Dissociation of the N-1–H bond in **1** would produce cytosine ***V***, which is 31 kJ mol^{-1} less stable than ***III***. Hence, the minimum energy path from **1** to ***V*** must involve energies of at least 31 kJ mol^{-1} higher than that for the threshold formation of ***III*** (130 kJ mol^{-1}) which is higher than **TS12** (154 kJ mol^{-1}). Other energetically competitive pathways for loss of H from **1** may involve isomerizations to radicals **5** or **6**, followed by dissociation through **TS16** and **TS17**, respectively. Although these

Table 4
Dissociation, ionization, recombination, and transition state energies of cytosine radicals

Reaction	Energy[a,b]		
	B3LYP/6-31+G(d,p)	B3-PMP2/6-311++G(3df,2p)	CCSD(T)[c]/6-311++G(3df,2p)
1 → **2**	54	51	48
1 → **3**	61	60	55
1 → **5**	31	36	31
1 → **6**	37	44	43
1 → **7a**	49	52	49
1 → **7b**	46	56	53
1 → **8a**	66	71	67
1 → **8b**	70	75	71
1 → **21**	177	203	190
1 → **22**	142	155	138
1 → $\mathbf{1}^+ + e^-$	509	503 (5.22)[d]	498 (5.17)[d]
1 → $\mathbf{1}^+ + e^-$ (vertical)		554 (5.74)[e]	
$\mathbf{1}^+ + e^-$ → **1** (vertical)		−455 (4.72)[f]	
2 → $\mathbf{2}^+ + e^-$	455	450 (4.66)[d]	445 (4.61)[e]
$\mathbf{2}^+ + e^-$ → **2** (vertical)		−403 (4.18)[f]	
3 → $\mathbf{3}^+ + e^-$	483	477 (4.95)[d]	475 (4.92)[e]
$\mathbf{3}^+ + e^-$ → **3** (vertical)		−428 (4.44)[f]	
1 → cytosine ***III*** + H	147	131	130
1 → cytosine ***V*** + H	176	161	161
2 → cytosine ***II*** + H	99	84	83
2 → cytosine ***III*** + H	93	80	82
3 → cytosine ***I*** + H	86	71	74
3 → cytosine ***V*** + H	115	101	105
1 → **23**	151	156	150
1 → **24**	163	169	164
1 → **25**	104	111	113
1 → **26**	71	67	82
1 → **27** + HN═C═O	235	240	246
1 → **28** + HN═C═O	242	240	244
1 → **29** + C═O	179	180	165
1 → **30** + C═O	159	166	147
1 → **TS12**	154	149	154
1 → **2** → **TS13**	171	171	182
2 → **TS13**	118	119	134
2 → **TS14**	114	111	121
3 → **TS15**	101	97	106
1 → **5** → **TS16**	152	144	148
1 → **6** → **TS17**	160	153	159
1 → **TS18**	159	167	168
1 → **TS19**	168	178	178
1 → **TS20**	108	119	127
1 → **TS21**	191	201	216
1 → **TS22**	172	182	169

[a] Energies in units of kJ mol^{-1}.
[b] Including B3LYP/6-31+G(d,p) zero-point energies and referring to 0 K.
[c] Effective energies from basis set expansion: E[CCSDT)/6–311++G(3df,2p)] = E[CCSDT)/6–31G(d,p)] + E[MP2/6-311++G(3df,2p)] − E[MP2/6–31G(d,p)].
[d] Adiabatic ionization energies in eV.
[e] Vertical ionization energies in eV.
[f] Vertical electron-ion recombination energies in eV.

TS are close in energy to **TS12**, the formation of intermediates **5** and **6** would require 1,3- and 1,2-hydrogen migrations through strained transition states. These usually require substantial TS energies in nucleobase radicals, e.g., >160 kJ mol^{-1} in adenine radicals [9], and may not be kinetically competitive with the direct loss of H-3 from **1**.

We conclude that loss of H from **1** through **TS12** appears to be the least-energy and thus kinetically preferred pathway.

Loss of a H-atom from **2** may involve dissociation of the O-2–H bond through **TS13** forming cytosine ***III***, or dissociation of the N-1–H bond through **TS14** forming cytosine ***II*** (Fig. 8). Of these, **TS14** occurs at a substantially lower energy and should be kinetically preferred. The activation energy for the loss of H-1 from **2** (E_a = 168.2−47.6 = 120.6 kJ mol^{-1}) is lower than that for the most facile loss of H from **1**. Thus, radical **2** is both thermodynamically and kinetically less stable than **1**. Vertical electron transfer to $\mathbf{2}^+$ is calculated to

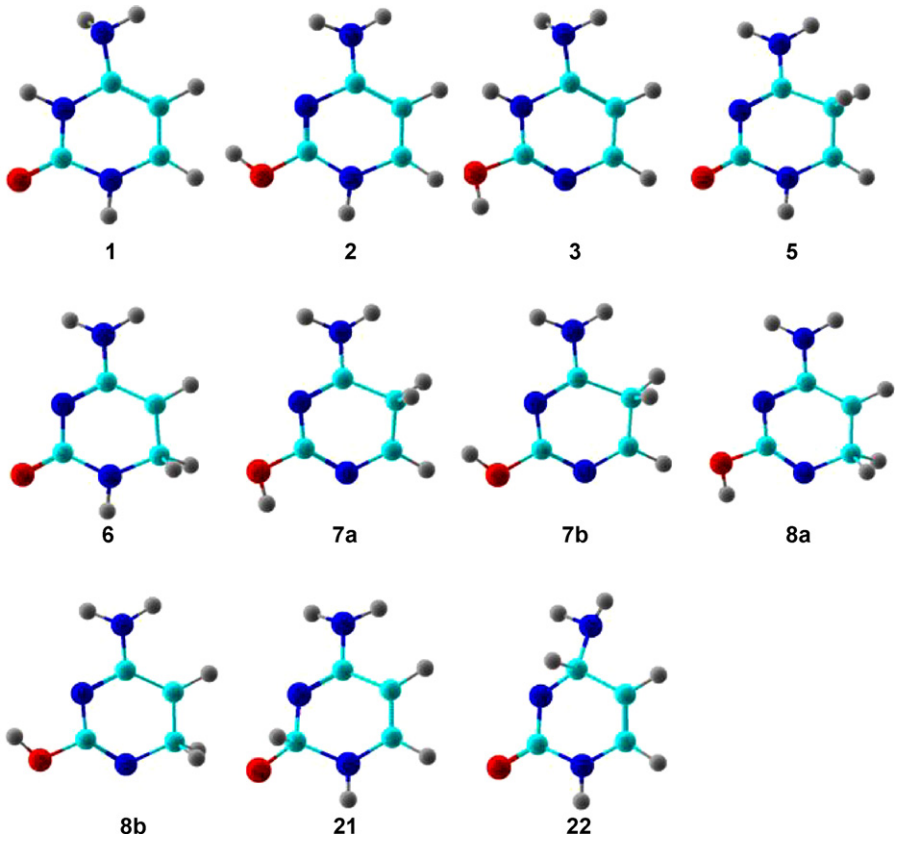

Fig. 7. B3LYP/6-31+G(d,p) optimized structures of [cytosine + H] radicals **1–3**, **5–8b**, **21**, and **22**.

produce **2** with $450-403=47\,\mathrm{kJ\,mol^{-1}}$ mean internal energy (Table 4), which is substantially less than the energy needed for dissociation. This indicates that a large fraction of vertically formed **2** should be thermodynamically stable and give rise to survivor ions in the $^{+}NR^{+}$ mass spectrum. Similar conclusions can be made for the loss of H atoms from radical **3** forming cytosine tautomers ***I*** and ***V*** (Table 4). The Franck-Condon energy in vertical electron transfer to $\mathbf{3}^{+}$ was calculated

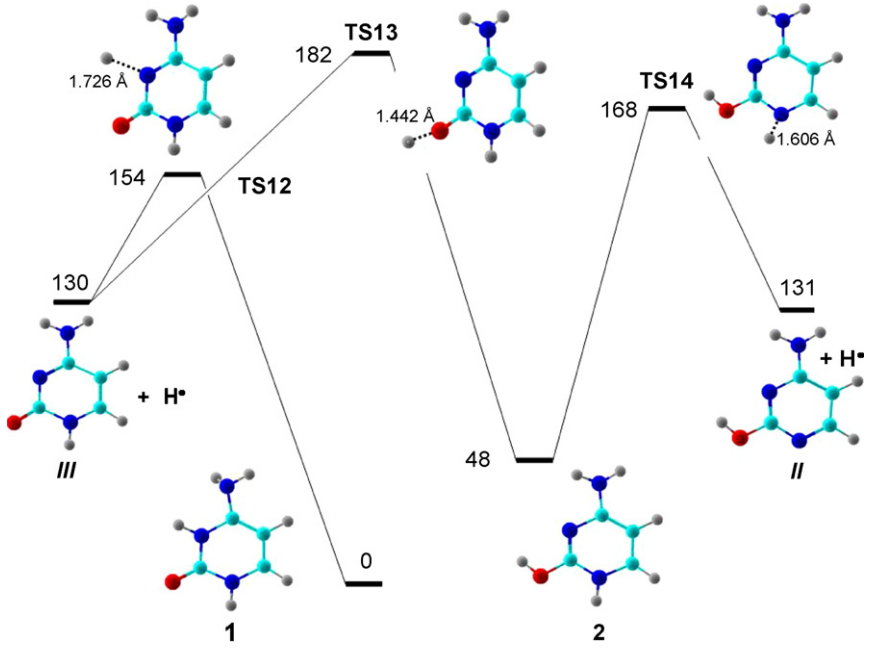

Fig. 8. Potential energy diagram for loss of H from [cytosine + H] radicals. Energies ($\mathrm{kJ\,mol^{-1}}$) are from effective CCSD(T)/6-311++G(3df,2p) single point calculations and include B3LYP/6-31+G(d,p) zero-point corrections.

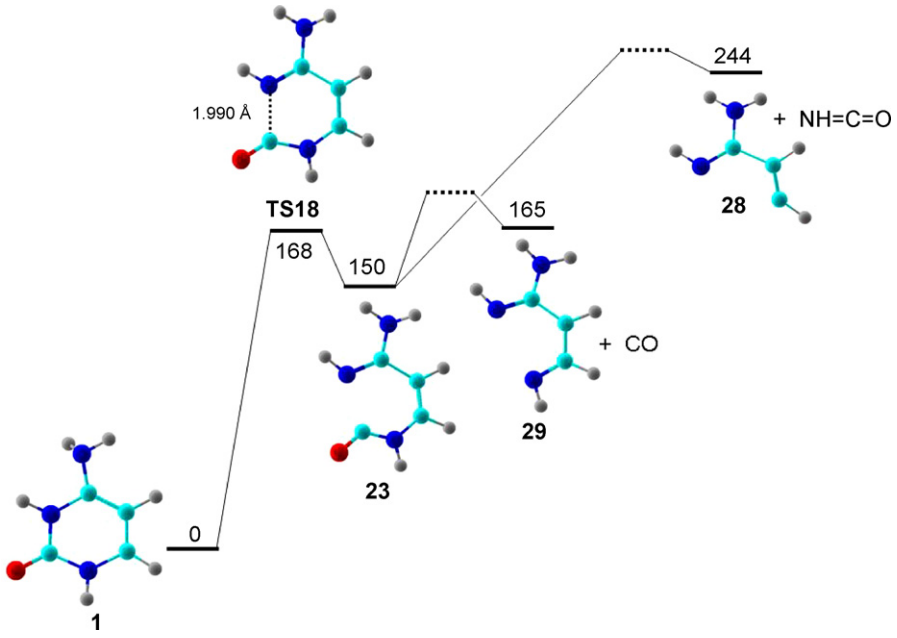

Fig. 9. Potential energy diagram for dissociations starting with the C-2—N-3 ring opening in [cytosine + H] radicals. Energies (kJ mol^{-1}) are from effective CCSD(T)/6-311++G(3df,2p) single-point calculations and include B3LYP/6-31+G(d,p) zero-point corrections.

to be 49 kJ mol^{-1}, which alone is insufficient to drive a dissociation.

It is worth noting that vertical ionization of **1**–**3** is also accompanied by Franck–Condon effects. Table 4 data indicate that the mean Franck–Condon energy in vertically formed $\mathbf{1}^+$ is 51 kJ mol^{-1}. The combined Franck–Condon energies in vertical neutralization and ionization (48 + 51 = 99 kJ mol^{-1}) result in an internal energy distribution in $\mathbf{1}^+$ which is broadened toward high energies [39,40] and promotes ion dissociations following reionization, as shown by the presence of consecutive dissociations by H losses in the $^+NR^+$ mass spectrum (Fig. 5a).

We have also used calculations to address ring-cleavage dissociations in **1** leading to the eliminations of CO and HNCO. Thus, cleavage of the C-2–N-3 bond in **1** proceeds through **TS18**, which is at 168 kJ mol^{-1} above **1** (Table 4, Fig. 9), to form an open-ring intermediate (**23**). The latter can eliminate CO to form radical **29** at 165 kJ mol^{-1} threshold energy. Overall this pathway may be competitive with the loss of H-3 from **1**,

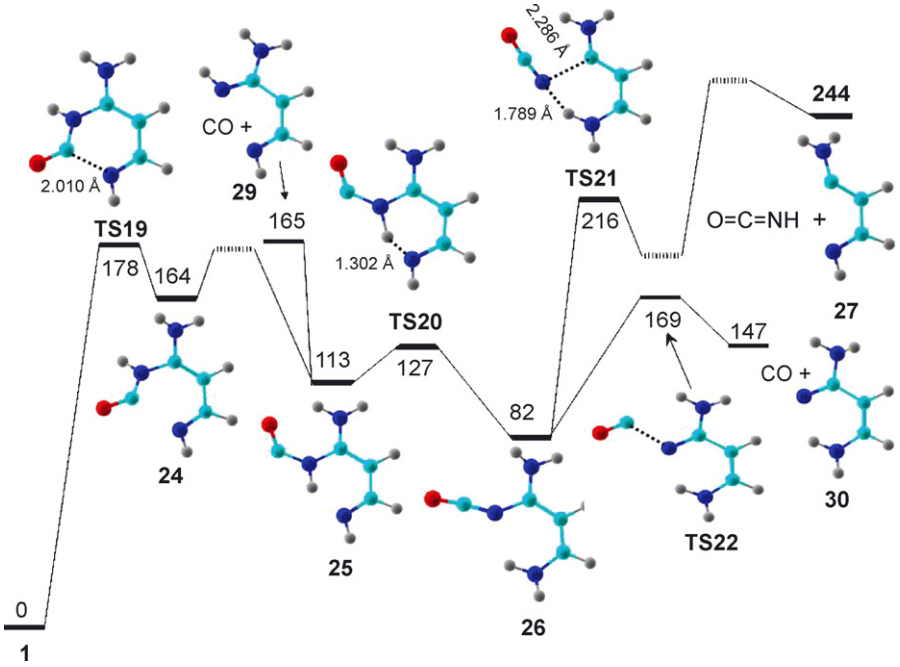

Fig. 10. Potential energy diagram for dissociations starting with the C-2—N-1 ring opening in [cytosine + H] radicals. Energies (kJ mol^{-1}) are from effective CCSD(T)/6–311++G(3df,2p) single-point calculations and include B3LYP/6-31+G(d,p) zero-point corrections.

barring a large barrier in the last step of CO loss, which we did not calculate. We note, however, that the expected peak of reionized **29**$^+$ at *m*/*z* 84 is rather weak in the $^+$NR$^+$ mass spectrum (Fig. 5a), indicating that the loss of CO is not very competitive. An elimination of HNCO from intermediate **23** requires 244 kJ mol^{-1} at the thermochemical threshold (Fig. 9), and may involve an additional barrier in the transition state. For energy reasons, the loss of HNCO from **1** does not appear to be competitive on the ground electronic potential energy surface of the system.

Cleavage of the C-2–N-1 bond in **1** produces somewhat more interesting chemistry (Fig. 10). After passing through **TS19** at 178 kJ mol^{-1} above **1**, the open-ring intermediate **24** can undergo cascade-like exothermic isomerizations, first to **25** by rotation about the N-3–C-4 bond, and then to **26** by hydrogen atom migration through **TS20**. These isomerizations require only relatively low-energy transition states and can occur spontaneously after the system passed through **TS19**. Intermediate **26** can eliminate CO through **TS22** to form radical **30** at 147 kJ mol^{-1} threshold energy. The competing elimination of HNCO requires a hydrogen atom migration in **TS21** and probably involves another intermediate, in which the HNCO molecule is hydrogen bonded to the incipient fragment **27**. However, the calculated threshold energy for the loss of HNCO (244 kJ mol^{-1}, Table 4), appears to be prohibitively high for this dissociation to compete with the loss of H. We note without proof that elimination of HNCO may proceed from an excited electronic state that was accessed by vertical electron transfer. Previous studies of uracil radicals indicated that up to 65% of all dissociations observed upon $^+$NR$^+$ could be ascribed to the involvement of excited electronic states [7,8]. Unfortunately, because of the complications with specific precursor-ion preparation, cytosine is not a suitable system for detailed mechanistic studies of neutral dissociations that would include excited electronic states.

4. Conclusions

This combined experimental and computational study allows us to arrive at the following conclusions. Protonation of cytosine is likely to produce mixtures of tautomeric cations, of which the most stable structures **1**$^+$ and **2**$^+$ differ by only 7 kJ mol^{-1}. Vertical electron transfer from trimethylamine to protonated cytosine produces a substantial fraction of stable radicals corresponding to hydrogen atom adducts to cytosine. The radicals in part dissociate by loss of H to reform cytosine tautomers. Quantum chemistry calculations are in accord that loss of H is the lowest energy dissociation of cytosine radicals. Alternative dissociations by ring cleavages and eliminations of CO and HNCO are not competitive on the potential energy surface of the ground electronic state of radicals **1**–**3**, but may proceeed from excited electronic states. The relative stabilities and dissociations energies of cytosine radicals are likely to be affected by solvation in water, as reported previously for *N*-methylcytosine [38], and also by hydrogen bonding in the DNA helix. In view of the substantial dissociation and transition state energies for unimolecular reactions of cytosine radicals, it appears that the condensed phase chemistry relevant to DNA damage will mainly involve bimolecular processes such as hydrogen transfer and redox reactions. Studies of these processes are in progress.

Acknowledgements

F.T. thanks the National Science Foundation for support through grants CHE-0349595 for experiments and CHE-0342956 for computations. The Computational Chemistry Center at the UW Department of Chemistry receives joint support by the NSF and University of Washington. C.W. thanks the NSF (CHE-0111128) for generous financial support. Thanks are due to Dr. Martin Sadilek for technical assistance with mass spectra measurements. The JEOL HX-110 mass spectrometer was a generous donation from the former Seattle Biomembrane Institute by courtesy of Professor S. Hakomori.

References

[1] C. Von Sonntag, The chemistry of free-radical-mediated DNA damage, in: W.A. Glass, M.N. Varma (Eds.), Physical and Chemical Mechanisms in Molecular Radiation Biology, Plenum Press, New York, 1991, p. 287.
[2] J.K. Wolken, F. Tureček, J. Phys. Chem. A 103 (1999) 6268.
[3] F. Tureček, J. Mass Spectrom. 33 (1998) 779.
[4] (a) P.M. Curtis, B.W. Williams, R.F. Porter, Chem. Phys. Lett. 65 (1979) 296;
(b) P.C. Burgers, J.L. Holmes, A.A. Mommers, J.K. Terlouw, Chem. Phys. Lett. 102 (1983) 1;
(c) P.O. Danis, C. Wesdemiotis, F.W. McLafferty, J. Am. Chem. Soc. 105 (1983) 7454.
[5] For recent reviews see;
(a) F. Turecek, Top. Curr. Chem. 225 (2003) 77;
(b) D.V. Zagorevskii, in: J.A. McCleverty, T.J. Meyer (Eds.), Comprehensive Coordination Chemistry II, Elsevier, Oxford, 2004, p. 381;
(c) F. Tureček, in: P.B. Armentrout (Ed.), Encyclopedia of Mass Spectrometry, vol. 1, Elsevier, Amsterdam, 2003, p. 528 (Chapter 7);
(d) D.V. Zagorevskii, Coord. Chem. Rev. 225 (2002) 5;
(e) P. Gerbaux, C. Wentrup, R. Flammang, Mass Spectrom. Rev. 19 (2000) 367;
(f) D.V. Zagorevskii, J.L. Holmes, Mass Spectrom. Rev. 18 (1999) 87;
(g) C. Schalley, G. Hornung, D. Schröder, H. Schwarz, Chem. Soc. Rev. 27 (1998) 91.
[6] J.K. Wolken, E.A. Syrstad, S. Vivekananda, F. Tureček, J. Am. Chem. Soc. 123 (2001) 5804.
[7] E.A. Syrstad, S. Vivekananda, F. Tureček, J. Phys. Chem. A 105 (2001) 8339.
[8] J.K. Wolken, F. Tureček, J. Phys. Chem. A 105 (2001) 8352.
[9] X. Chen, E.A. Syrstad, M.T. Nguyen, P. Gerbaux, F. Tureček, J. Phys. Chem. A 109 (2005) 8121.
[10] C. Yao, M. Cuadrado-Peinado, M. Polášek, F. Tureček, Angew. Chem. Int. Ed. Engl. 44 (2005) 6708.
[11] C. Yao, M. Cuadrado-Peinado, M. Polášek, F. Tureček, J. Mass Spectrom. 40 (2005) 1417.
[12] J. Wu, C. Wesdemiotis, J. Am. Soc. Mass Spectrom. 12 (2001) 1229.
[13] M.J. Polce, M.M. Cordero, C. Wesdemiotis, P.A. Bott, Int. J. Mass Spectrom. Ion Processes 113 (1992) 35.
[14] M.J. Polce, S. Beranova, M.J. Nold, C. Wesdemiotis, J. Mass Spectrom. 31 (1996) 1073.
[15] D. Schröder, in: P.B. Armentrout (Ed.), The Encyclopedia of Mass Spectrometry, vol. 1, 2003, pp. 521–528 (Chapter 8).
[16] M.J. Frisch, et al., Gaussian 03, Revision B.05; Gaussian, Inc., Pittsburgh, PA, 2003.
[17] A.D. Becke, J. Chem. Phys. 98 (1993) 1372.
[18] A.D. Becke, J. Chem. Phys. 98 (1993) 5648.

[19] P.J. Stephens, F.J. Devlin, C.F. Chabalowski, M.J. Frisch, J. Phys. Chem. 98 (1994) 11623.
[20] C. Møller, M.S. Plesset, Phys. Rev. 46 (1934) 618.
[21] F. Tureček, C.J. Cramer, J. Am. Chem. Soc. 117 (1995) 12243.
[22] T.H. Dunning Jr., J. Chem. Phys. 90 (1989) 1007.
[23] F. Tureček, J. Phys. Chem. A 102 (1998) 4703.
[24] (a) F. Tureček, M. Polášek, A.J. Frank, M. Sadílek, J. Am. Chem. Soc. 122 (2000) 2361;
(b) M. Polášek, F. Tureček, J. Am. Chem. Soc. 122 (2000) 9511;
(c) P.R. Rablen, J. Am. Chem. Soc. 122 (2000) 357;
(d) P.R. Rablen, J. Org. Chem. 65 (2000) 7930;
(e) P.R. Rablen, K.H. Bentrup, J. Am. Chem. Soc. 125 (2003) 2142;
(f) M. Hirama, T. Tokosumi, T. Ishida, J. Aihara, Chem. Phys. 305 (2004) 307;
(g) Y.M.E. Fung, H. Liu, T.W.D. Chan, J. Am. Soc. Mass Spectrom. 17 (2006) 757.
[25] J. Čížek, J. Paldus, L. Šroubková, Int. J. Quantum Chem. 3 (1969) 149.
[26] G.D. Purvis, R.J. Bartlett, J. Chem. Phys. 76 (1982) 1910.
[27] F. Tureček, in: J.S. Splitter, F. Turecek (Eds.), Applications of Mass Spectrometry to Organic Stereochemistry, VCH Publishers, New York, 1994 (Appendix 1).
[28] (a) J. Šponer, P. Hobza, Collect. Czech. Chem. Commun. 68 (2003) 2231;
(b) M. Szczesniak, K. Szczepaniak, J.S. Kwiatkowski, K. Kubulat, W.B. Person, J. Am. Chem. Soc. 110 (1988) 8319.
[29] Y. Podolyan, L. Gorb, J. Leszczynski, J. Phys. Chem. A 104 (2000) 7346.
[30] A.K. Chandra, M.T. Nguyen, T. Zeegers-Huyskens, J. Mol. Struct. 519 (2000) 1.
[31] (a) S. Kabli, E.S.E. Van Beelen, S. Ingemann, L. Henriksen, S. Hammerum, Int. J. Mass Spectrom. 249 (2006) 370;
(b) T.A. Van Beelen, S. Koblenz, L. Ingemann, S. Henriksen, Hammerum, J. Phys. Chem. A 108 (2004) 2787;
(c) S. Hammerum, T.I. Solling, J. Am. Chem. Soc. 121 (1999) 6002;
(d) S. Hammerum, Chem. Phys. Lett. 300 (1999) 529.
[32] (a) J.W. Larson, T.B. McMahon, J. Am. Chem. Soc. 104 (1982) 6255;
(b) M. Mautner, J. Am. Chem. Soc. 106 (1984) 1257;
(c) V.Q. Nguyen, F. Tureček, J. Mass Spectrom. 31 (1996) 1173.
[33] NIST Standard Reference Database No. 69. June 2005 release. http://webbook.nist.gov/chemistry.
[34] F. Tureček, X. Chen, J. Am. Soc. Mass Spectrom. 16 (2005) 1713.
[35] H. Cao, Y. Wang, J. Am. Soc. Mass Spectrom. 17 (2006) 1335.
[36] F. Tureček, D.E. Drinkwater, F.W. McLafferty, J. Am. Chem. Soc. 112 (1990) 993.
[37] J.D. Zhang, Y. Xie, H.F. Schaefer, Q. Luo, Q.-S. Li, Mol. Phys. 104 (2006) 2347.
[38] F. Tureček, C. Yao, J. Phys. Chem. A 107 (2003) 9221.
[39] V.Q. Nguyen, F. Tureček, J. Mass Spectrom. 31 (1996) 843.
[40] S. Beranova, C. Wesdemiotis, J. Am. Soc. Mass Spectrom. 5 (1994) 1093.